A Model Predictive Control Approach for Path Following and Evasive Manoeuvres in the Realm of Vehicle Motion Control

Petar Velchev, Floris van Leeuwen,

***Abstract*—A model predictive control (MPC) approach is studied for motion control of vehicles, specifically that of path following during aggressive obstacle avoidance manoeuvres. The proposed MPC framework integrates a predictive model of vehicle dynamics with optimization to generate control inputs that steer the simulated non-linear vehicle along a desired path while efficiently avoiding obstacles. Through extensive simulation and validation, the effectiveness of the MPC approach in achieving robust and agile motion control can be demonstrated, even in challenging manoeuvres such as the industry standard *Elk Test*. The results highlight the potential of MPC for ensuring the safety and agility of autonomous vehicles in safety critical driving scenarios.**

I. Introduction

The advancements in autonomous driving have drastically changed the current transportation landscape and will likely continue to do so for the next decades. Central to this development is the implementation of robust control strategies that enable precise path following and allow for effective navigation through dynamic environments.

One essential part of this process, is the guarantee that the vehicle can perform evasive manoeuvres such as obstacle avoidance without risking passenger safety. Therefore, a model predictive control approach is studied for motion control of vehicles in varying path following scenarios.

As a vehicle is bounded by physical limits, most classical control strategies such as LQR won't be able to handle these restraints related to state dynamics and inputs. MPC is a powerful control framework that is able to handle these constraints and optimize control actions for a finite prediction horizon while retaining stability guarantees. It presents itself as an optimal choice for such autonomous driving scenarios.

The proposed MPC approach leverages the dynamic bicycle model as a prediction model to capture both the lateral and longitudinal dynamics of the vehicle without risking overcomplicating the model. The MPC approach will undergo several alterations throughout this report to optimize for varying scenarios, such as disturbance rejection and prediction model extensions.

Petar Velchev and Floris van Leeuwen are master students at TU Delft, The Netherlands. E-mail addresses: {P.A.Velchev, F.N.vanLeeuwen}@student.tudelft.nl.

A. Prediction Model

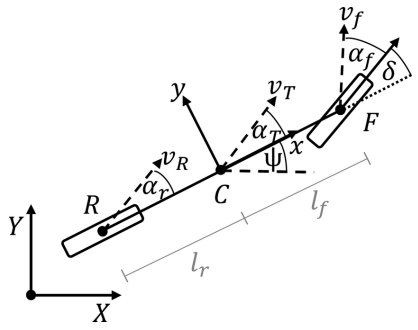

Fig. 1. Dynamic bicycle model [1]

The prediction model is based on the linear dynamic bicycle model, shown in figure 1, which equations have been derived from the work presented in article [2] by J.M. Snider.

Reducing the complexity of large vehicle models to a less complex version such as the kinematic and dynamic bicycle model is common practice for scenarios involving motion planning and deriving intuitive control laws. The dynamic bicycle model simplifies the vehicles structure to a 2 wheel base, hence its name, structured as a set of interconnected components, which includes parts as the frame, wheels, steering mechanism, etc. This allows to simulate how the vehicle would respond to various inputs such as steering angle and braking.

Its usability in this scenario relies on the fact that the model is capable of capturing both lateral dynamics, which describe the motion of the vehicle in the horizontal plane such as lane changes, and longitudinal dynamics, which relate to motion along the direction of travel.

The system states are position y, lateral velocity v_y, yaw ψ and yaw rate r respectively, and the system input is given by delta δ, which relates to the steering angle. The dynamics are governed by the following equations:

$$\begin{aligned} \dot{x} &= Ax + Bu \\ y &= Cx + Du, \end{aligned} \tag{1}$$

Where the state matrix A is given by:

$$A = \begin{bmatrix} 0 & 1 & 0 & 0 \\ 0 & -\frac{Ca_f + Ca_r}{m \cdot V_x} & \frac{Ca_f + Ca_r}{m} & -\frac{l_f \cdot Ca_f - l_r \cdot Ca_r}{m \cdot v_x} \\ 0 & 0 & 0 & 1 \\ 0 & -\frac{l_f \cdot Ca_f - l_r \cdot Ca_r}{I_{zz} \cdot v_x} & \frac{l_f \cdot Ca_f - l_r \cdot Ca_r}{I_{zz}} & -\frac{l_f^2 \cdot Ca_f + l_r^2 \cdot Ca_r}{I_{zz} \cdot v_x} \end{bmatrix}$$

And vectors B, C and D are given by:

$$B = \begin{bmatrix} 0 \\ \frac{Ca_f}{m} \\ 0 \\ \frac{l_f \cdot Ca_f}{I_{zz}} \end{bmatrix}, \quad C^T = \begin{bmatrix} 1 \\ 0 \\ 0 \\ 0 \end{bmatrix}, \quad D = 0$$

The parameters can be found in table I. Further in the report, the system will undergo an extension to handle disturbances, which will be covered in section II-A.

TABLE I
VEHICLE PARAMETERS

Parameter	Value
Gravity acceleration, g (m/s^2)	9.81
Distance from front axle to CoG, l_f (m)	1.40
Distance from rear axle to CoG, l_r (m)	1.45
Wheelbase, L (m)	2.80
Vehicle mass, m (kg)	1950
Inertia moment about vertical axis, I_{zz} (kg·m^2)	2000
Front axle cornering stiffness, C_{a_f} (N/rad)	2×92000
Rear axle cornering stiffness, C_{a_r} (N/rad)	2×97000
Steering ratio, u_{steer}	17.5
Vehicle side slip angle, β (rad)	$\frac{15\pi}{180}$

B. The plant

The decision has been made to adopt for a nonlinear dynamic bicycle model as the plant. This choice prevents the utilization of the same model for both prediction and system, thereby creating a more realistic modeling environment.

The equations for the plant have been derived from the work presented in the paper [3] by N. Chowdhri. The model extends the prediction model with 2 states, representing longitudinal position x and velocity v_x. It is noteworthy that the longitudinal velocity is held constant in the prediction model. The dynamics are governed by the following equations:

$$\begin{aligned} \dot{v_x} &= v_y \cdot r \\ \dot{v_y} &= -\left(\frac{C_{a_f} + C_{a_r}}{m \cdot v_x}\right) \cdot v_y \\ &\quad + \left(\frac{l_r \cdot C_{a_r} - l_f \cdot C_{a_f}}{m \cdot v_x} - v_x\right) \cdot r + \frac{C_{a_f}}{m} \cdot \delta \\ \dot{r} &= \left(\frac{l_r \cdot C_{a_r} - l_f \cdot C_{a_f}}{I_{zz} \cdot v_x}\right) \cdot v_y \\ &\quad + \left(-\frac{l_r^2 \cdot C_{a_r} + l_f^2 \cdot C_{a_f}}{I_{zz} \cdot v_x}\right) \cdot r + \frac{l_f \cdot C_{a_f}}{I_{zz}} \cdot \delta \\ \dot{\psi} &= r \\ \dot{x}_p &= v_x \cdot \cos(yaw) - v_y \cdot \sin(yaw) \\ \dot{y}_p &= v_x \cdot \sin(yaw) + v_y \cdot \cos(yaw) \end{aligned} \tag{2}$$

C. Reference generator

The references used for testing the models were derived from realistic scenarios that are commonly used to evaluate vehicle performance. The first reference is based on a lane change manoeuvre. The lane change course comprises a straight section of a two-lane road where the vehicle executes a double lane change. After the initial lane change, the vehicle continues straight for some distance before returning to its original lane, resembling a typical overtaking manoeuvre.

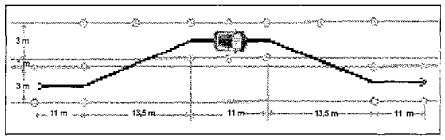

Fig. 2. Moose test [4]

The second reference is based on the moose test, which originated from Sweden in 1970 due to the high amount of collisions with animals, particularly moose. This scenario simulates an abrupt swerving manoeuvre to avoid a potential collision with an unexpected obstacle on the road. The path is similar to that of the lane change , but clearly distinguishable by its emphasis on abrupt and aggressive manoeuvring. The designed reference would oppose a real challenge for any real or simulated vehicle.

D. Discrete dynamics

The prediction model is discretized using a zero-order hold approach with a sampling time of 0.1 seconds. This process is done by using the `c2d` function in MATLAB, resulting in the following dynamic model:

$$\begin{aligned} x_{k+1} &= \Phi x_k + \Gamma u_k \\ y_k &= C x_k + D u_k \end{aligned} \tag{3}$$

Subsequently, the nonlinear plant undergoes discretization by leveraging the `ode45` function in MATLAB by solving the dynamics for a single step.

II. MODEL PREDICTIVE CONTROL DESIGN

Based on the dynamical models derived in section I the following MPC controllers were designed to achieve the desired obstacle avoidance vehicle motion:

1) Full information state feedback reference tracking MPC for an undisturbed system.
2) Output MPC reference tracking with Optimal Target Selection and Disturbance Rejection.

For both designs, the control action (steering angle at the wheels) is bound by the physical actuation limits of the steering rack and respective suspension geometry as follows:

$$\begin{bmatrix} 1 \\ -1 \end{bmatrix} u_k \leqslant \begin{bmatrix} 0.35 \\ 0.35 \end{bmatrix} \tag{4}$$

Similarly, the state constraints follow from physical limits being imposed on the vehicle model and its environment.

The position is constrained by the width of a standard road, keeping in mind that the vehicle drives in the center of a lane rather than road center. The lateral velocity is constrained by a combination of the permissible side-slip angle and longitudinal velocity, which value can be seen in table I. Lastly the yaw rate is bounded as to not spin the vehicle, it can be noted that this constraint can be tightened for passenger comfort or prolonged longevity of the actuator system used in yaw rate control, such as the brake system.

$$M = \begin{bmatrix} -2 \\ -\beta \\ -10 \\ -2 \end{bmatrix} \leqslant \begin{bmatrix} y_k \\ vy_k \\ \psi_k \\ r_k \end{bmatrix} \leqslant \begin{bmatrix} 5 \\ \beta \\ 10 \\ 2 \end{bmatrix} = T \tag{5}$$

The above constraints can be compactly combined in $Fx(k) \leq e$ as follows:

$$F = \begin{bmatrix} I \\ -I \end{bmatrix}, \quad e = \begin{bmatrix} T \\ -M \end{bmatrix} \tag{6}$$

Furthermore, the cost function is defined as:

$$\begin{gathered} J\left(x_0, u\right) = \sum_{k=0}^{N-1} \ell(x_k, u_k) + V_f(x_N) \\ \text{s.t. } x \in \mathbb{X}, u \in \mathbb{U}, x_N \in \mathbb{X}_f \end{gathered} \tag{7}$$

Where the stage $\ell(x_k, u_k)$ and terminal costs $V_f(x_N)$ are given by:

$$\begin{aligned} \ell(x_k, u_k) &= \frac{1}{2} x_k^T Q x_k + u_k^T R u_k \\ V_f(x_N) &= \frac{1}{2} x_N^T \, \mathrm{P} \, x_N \end{aligned} \tag{8}$$

With matrices $Q = 100\text{diag}(500, 1, 8, 40) \geq 0$, $R = 0.1I$ and P is the solution of the discrete time Algebraic Riccati Equation (DARE).

The full information state feedback tracking controller makes use of the discrete dynamics introduced in section I and availability of all state measurements. For report conciseness, the full information reference tracking controller is omitted as it is a sense simplified version of the output controller with disturbance rejection. The following section thus focuses on the design of the latter.

A. Output tracking and disturbance rejection

In the domain of vehicle dynamics, it is often the case that direct state measurement via sensors is not possible. This serves as motivation for an output controller for reference tracking with disturbance rejection and state estimation. Assuming that the vehicle lateral position can be measured using a system such as computer vision from a camera, the remaining vehicle states are estimated through state-space augmentation and Kalman filtering as follows:

$$\begin{aligned} x_{k+1} &= \tilde{\Phi} x_k + \tilde{\Gamma} u_k + \tilde{\Gamma}_d d_k \\ y_k &= C x_k + D u_k \end{aligned} \tag{9}$$

$$\begin{aligned} \begin{bmatrix} x_{k+1} \\ d_{k+1} \end{bmatrix} &= \begin{bmatrix} \Phi & \Gamma_d \\ 0 & I \end{bmatrix} \begin{bmatrix} x_k \\ d_k \end{bmatrix} + \begin{bmatrix} \Gamma \\ 0 \end{bmatrix} u + \begin{bmatrix} w \\ w_d \end{bmatrix} \\ y_k &= \begin{bmatrix} C & C_d \end{bmatrix} \begin{bmatrix} x_k \\ d_k \end{bmatrix} + v \end{aligned} \tag{10}$$

The Γ_d and C_d matrices are used to impose a dynamic disturbance (but constant throughout the prediction horizon) on the lateral position state, simulating a perpendicular wind gust force acting on the vehicle. For this, it is checked that the original system pair (Φ, C) is observable and furthermore:

$$\operatorname{rank} \begin{bmatrix} I - \Phi & -\Gamma_d \\ C & C_d \end{bmatrix} = n + n_d = 4 + 1 = 5 \tag{11}$$

The optimal target selection (OTS) is solved online to find the needed x_{ref} and u_{ref}, which can in turn reject the disturbances acting on the respective state.

$$\begin{gathered} \left(x_{\text{ref}}, u_{\text{ref}}\right) \left(\hat{d}, y_{\text{ref}}\right) \in \\ \begin{cases} \arg\min_{x_r, u_r} J\left(x_r, u_r\right) \\ \text{s.t. } \begin{bmatrix} I - \Phi & -\Gamma \\ C & 0 \end{bmatrix} \begin{bmatrix} x_r \\ u_r \end{bmatrix} = \begin{bmatrix} \Gamma_d \hat{d} \\ y_{\text{ref}} - C_d \hat{d} \end{bmatrix} \\ \left(x_r, u_r\right) \in \mathbb{Z} \\ C x_r + d \in \mathbb{Y} \end{cases} \end{gathered} \tag{12}$$

The above OTS solves for the reference signals x_{ref} and u_{ref}, and thus the objective function for the reference tracking optimal control action is derived.

$$\begin{aligned} \ell(x_k, u_k) &= \frac{1}{2} \left(x_k - x_{\text{ref}}\right)^T Q \left(x_k - x_{\text{ref}}\right) \\ &\quad + \left(u_k - u_{\text{ref}}\right)^T R \left(u_k - u_{\text{ref}}\right) \\ V_f(x_N) &= \frac{1}{2} \left(x_N - x_{\text{ref}}\right)^T P \left(x_N - x_{\text{ref}}\right) \end{aligned} \tag{13}$$

Lastly, the Kalman filter used as observer is implemented with weighing matrices $Q_K = 110I$ and $R = 90I$ such that the observer error dynamics converge quicker than the closed loop convergence. The resulting controller formulation with Kalman gain K is then:

$$\begin{aligned} \begin{bmatrix} \hat{x}_{k+1} \\ \hat{d}_{k+1} \end{bmatrix} &= \tilde{\Phi} \begin{bmatrix} \hat{x}_k \\ \hat{d}_k \end{bmatrix} + \begin{bmatrix} \Gamma \\ 0 \end{bmatrix} u_k + K \left(y - \tilde{C} \begin{bmatrix} \hat{x}_k \\ \hat{d}_k \end{bmatrix} \right) \\ \tilde{\Phi} &= \begin{bmatrix} \Phi & \Gamma_d \\ 0 & I \end{bmatrix}, \tilde{C} = \begin{bmatrix} C & C_d \end{bmatrix} \end{aligned} \tag{14}$$

B. Terminal Set

The Terminal Set $\mathbb{X}_f$ is designed to be a control invariant set and forms the foundation for the asymptotic stability analysis to follow. The set $\mathbb{X}_f$ was found by utilization of the MPT3 toolbox for Matlab and respective invariantSet() command. This resulted in a terminal set in the fourth dimension comprised of 32 linear inequalities, satisfying the relation:

$$\mathbb{X}_f = \left\{ x \in \mathbb{R}^4 \mid Ax \leq b \right\} \tag{15}$$

The terminal set is depicted in Figure 3, projected into the 2D space of the lateral position and yaw angle states.

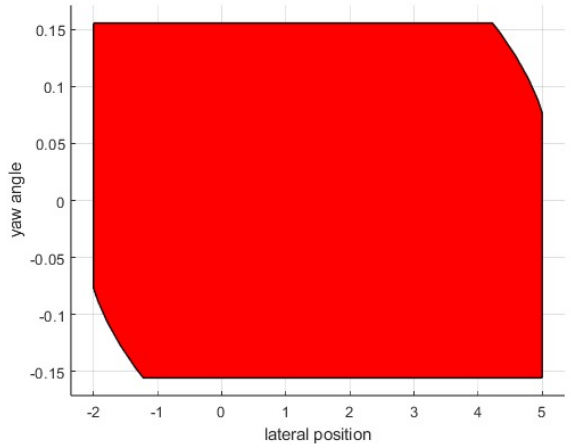

Fig. 3. Terminal Set projected onto a 2D state space.

The Lyapunov decrease condition:

$$V_f(f(x,u)) - V_f(x) \leq -\ell(x,u), \tag{16}$$

which is discussed in the asymptotic stability analysis was verified analytically as shown in Figure 4 below.

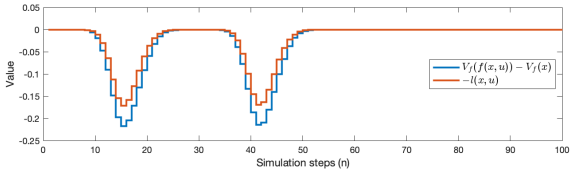

Fig. 4. Verification of Assumption 2.14 condition on the cost function decrease.

III. Asymptotic Stability

In this section, the asymptotic stability of the designed MPC closed-loop system is analyzed. This is done through validation of Theorem 2.19 of the book [5] as shown below and respective assumptions.

Theorem 2.19 (Asymptotic stability of the origin). Suppose Assumptions 2.2, 2.3, 2.14, and 2.17 are satisfied. Then

(a) There exists $\mathcal{K}_\infty$ functions $\alpha_1(\cdot)$ and $\alpha_2(\cdot)$ such that for all $x \in X_N$ $\left(\bar{X}_N^c\right.$, for each $c \in \mathbb{R}_{>0}$ $)$

$$\alpha_1(|x|) \leq V_N^0(x) \leq \alpha_2(|x|)$$
$$V_N^0\left(f\left(x, \kappa_N(x)\right)\right) - V_N^0(x) \leq -\alpha_1(|x|)$$

(b) The origin is asymptotically stable in χ_N $\left(\bar{X}_N^c\right.$, for each $c \in \mathbb{R}_{>0}$ $)$ for $x^+ = f\left(x, \kappa_N(x)\right)$.

As stated, Theorem 2.19 relies on the following assumptions to hold to prove asymptotic stability of the origin. Each assumption will be individually covered as follows:

Assumption 2.2 (Continuity of system and cost). The functions $f\colon \mathbb{Z} \to \mathbb{X}, \ell\colon \mathbb{Z} \to \mathbb{R}_{\geq 0}$ and $V_f\colon \mathbb{X}_f \to \mathbb{R}_{\geq 0}$ are continuous, $f(0,0) = 0, \ell(0,0) = 0$ and $V_f(0) = 0$.

From the dynamics derived in section I, the function $f(x,u)$ is seen to be null for zero valued inputs as well as continuous, also proven by its linearity. Furthermore, the cost function comprising of the stage cost $\ell(x,u)$ and terminal cost $V_{\mathrm{f}}(x)$ are both continuous and quadratic with $\ell(0,0) = 0$ and $V_f(0) = 0$ 7. Namely, $\ell(x,u) \geq 0$ and $V_f(x) \geq 0$ for $Q, R, P > 0$.

Assumption 2.3 (Properties of constraint sets). The set $\mathbb{Z}$ is closed and the set $\mathbb{X}_f \subseteq \mathbb{X}$ is compact. Each set contains the origin. If $\mathbb{U}$ is bounded (hence compact), the set $\mathbb{U}(x)$ is compact for all $x \in \mathbb{X}$. If $\mathbb{U}$ is unbounded, the function $\mathbf{u} \mapsto V_N(x,\mathbf{u})$ is coercive, i.e., $V_N(x,\mathbf{u}) \to \infty$ as $|\mathbf{u}| \to \infty$ for all $x \in \mathbb{X}$).

It follows by definition from section II-B that sets $\mathbb{U}$ and $\mathbb{X}_f$ are compact since they are closed and bounded. This is shown by the fact that $\mathbb{X}_f$ is bounded by linear inequalities and the control action was bounded by the physical actuation limits of the steering system and suspension geometry. Lastly it can be seen that that $\mathbb{X}_f \subseteq \mathbb{X}$ in figure 3. Both $\mathbb{X}_f$ and $\mathbb{U}$ contain the origin.

Assumption 2.14 (Basic stability assumption). $V_f(\cdot), \mathbb{X}_f$ and $\ell(\cdot)$ have the following properties: (a) For all $x \in \mathbb{X}_f$, there exists a u (such that $(x,u) \in \mathbb{Z}$) satisfying

$$f(x,u) \in \mathbb{X}_f$$
$$V_f(f(x,u)) - V_f(x) \leq -\ell(x,u)$$

(b) There exist $\mathcal{K}_\infty$ functions $\alpha_1(\cdot)$ and $\alpha_f(\cdot)$ satisfying

$$\ell(x,u) \geq \alpha_1(|x|) \forall x \in X_N, \forall u \text{ such that } (x,u) \in \mathbb{Z}$$
$$V_f(x) \leq \alpha_f(|x|) \forall x \in \mathbb{X}_f$$

Part a) of assumption 2.14 is proven by figure 4, which shows that $V_f(f(x,u)) - V_f(x)$ stays below or is equal to the threshold of the negative stage cost $-\ell(x,u)$. Part b) can be proven by carefully selecting the function for $\alpha_1(|x|)$ and $\alpha_1 f(|x|)$, which guarantees the constraint to hold.

$$\ell(x,u) \geq \frac{1}{2}\lambda_{\min}(Q)|x|^2 = \alpha_1(|x|) \qquad \forall x \in \mathcal{X}_N$$
$$V_f(x) \leq \frac{1}{2}\lambda_{\max}(P)|x|^2 = \alpha_f(|x|) \qquad \forall x \in \mathbb{X}_f$$

Assumption 2.17 (Weak controllability). There exists a $\mathcal{K}_\infty$ function $\alpha(\cdot)$ such that

$$V_N^0(x) \leq \alpha(|x|) \forall x \in X_N$$

The system's controllability has been verified through a full rank controllability matrix, proving a more rigorous level of control. This automatatically validates the assumption.

By having proven assumptions 2.2, 2.3, 2.14, and 2.17, it can be asserted that, in accordance with theorem 2.19, the system is asymptotically stable at the origin.

IV. Numerical simulations

In this section, the numerical simulations of controllers proposed in section II will be discussed.

A. Reference tracking

Firstly, the system was simulated with full state information for reference tracking without disturbance rejection. This was partially done to simplify of the system, but also to find a baseline of performance, specifically with regards to tuning. The performance of the simulated system for a double lane change is depicted in Figure 5. Even though specific Key Performance Indicators (KPIs) are not evaluated, it can be seen that the system achieves accurate tracking for the required manoeuvre, in fact more than sufficient for a real world scenario overtake.

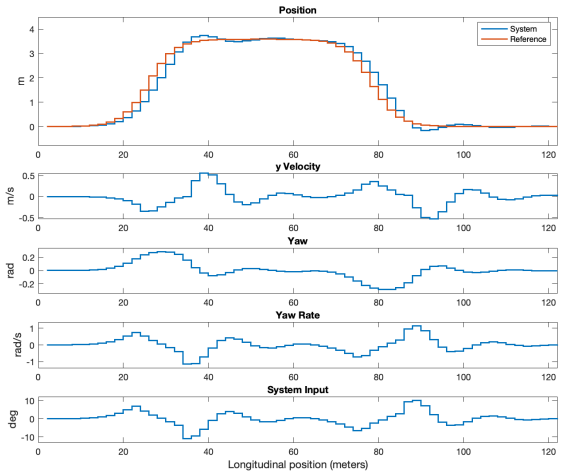

Fig. 5. States and system input lane change

The performance from a simulated Moose test manoeuvre is depicted in Figure 6. As this type of evasive manoeuvre is geometrically more aggressive, it is in line with the expectations that more non-linear behaviour of the plant will be triggered resulting in more overall overshoot and longer duration of the transients.

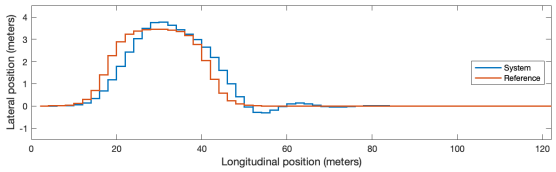

Fig. 6. Moose test position

Figure 11 shows the lane change performance for a range of prediction horizon lengths. As this project omits the path planning component of autonomous driving, the full reference trajectory for the lane change is provided at every iteration of the control application as discussed previously. The effects of this can be seen in that short horizon lengths, where the controller does not have enough look-ahead yielding to poor tracking performance. On the other hand, due to the large sampling time of 0.1s, too long of a horizon length can also degrade tracking performance as a large portion of the steady state of the manouevre influences the control action.

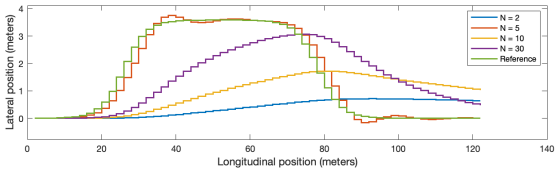

Fig. 7. Lane change performance for a range of prediction horizons.

B. Disturbance rejection

The augmented system for disturbance rejection was simulated with a stepped varying disturbance on the lateral position state. In real life this can be explained by a perpendicular force acting on the vehicle as a disturbance due to side wind. The performance for the system is shown in Figure 8, where it can be seen that the system is affected by the disturbance with slight overshoot in both the transient and steady state portion of the double lane change, but recovers to zero steady state error.

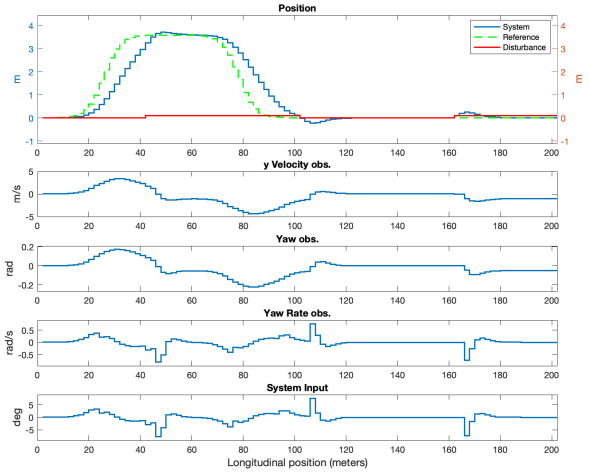

Fig. 8. System augmentation with disturbance rejection

Next, the disturbed system was simulated on the more aggressive Moose test geometry as depicted in Figure 9. Here it can be seen that the performance is slightly worse in terms of tracking error compared to the nominal reference tracking discussed previously. This can be explained by the fact that the cost function turning of this controller is slightly more relaxed, in order to achieve faster convergence of the observer.

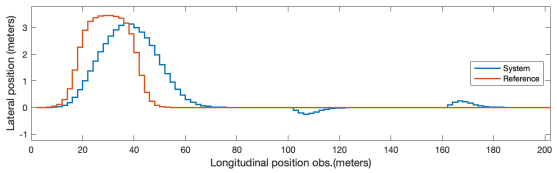

Fig. 9. Moose test for system augmentation with disturbance rejection.

Figure 10 shows the control action and disturbance signal on the lateral position. This verifies a slightly delayed steering input following from the step increase of the disturbance signal resulting in elimination of the steady state offset which would otherwise occur.

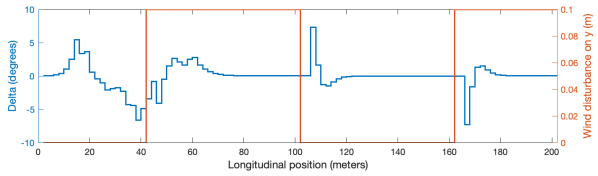

Fig. 10. Control action of moose test for system augmentation with disturbance rejection.

C. Input modification

As a final experiment, the system was modified to have a second input to the system, in line with the dynamic bicycle model discussed in the article [2] by J.M. Snider. Additionally, the system now incorporates control over the yaw rate as a second input alongside the steering angle, thereby evolving the system into a Multiple-Input Single-Output (MISO) system. Due to time constraints, the model was tested with prediction model and system being identical and relaxed constraints to see how far the system could be pushed. This resulted in almost perfect reference tracking for the Moose test but rather unrealistic for real life scenarios.

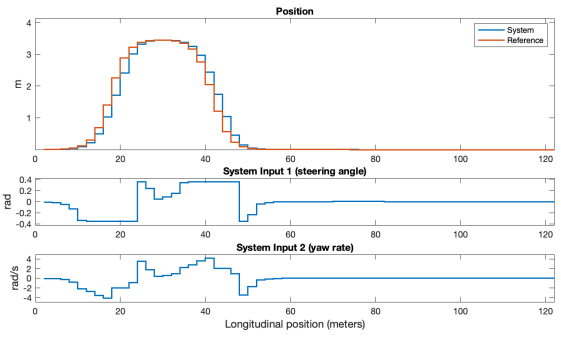

Fig. 11. Modified system with 2 inputs

D. Video Simulation

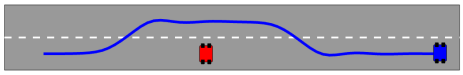

To view the reference tracking simulation, please click here: Lane change

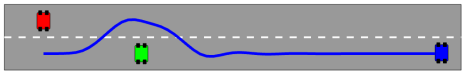

To view the moose test simulation, please click here: Moose test

V. Conclusion

This report summarizes the successful design and implementation of an MPC controller for path following of vehicle motion control in the domain of evasive manoeuvres.

It has been shown that the linear bicycle vehicle model simplification used for the predictive model of the MPC controller is sufficient to drive a non-linear vehicle plant simulation, albeit with simple tire modelling. It is therefore recommended as future work to firstly investigate the complexity of the vehicle plant. This can be done through implementing a high fidelity dual track vehicle model as well as dynamic tire models such as a Brush, Dughoff or Magic formula tire model.

Secondly, more time can be spent on the tuning of the observer such that the accuracy of the estimated disturbance is improved.

Lastly, a first step was made to control the system with a second control action. This can be extended further to include the incorporation of stability control via use the the brake system actuation as well as rear-wheel steering for a larger vehicle dynamics performance envelope.

References

[1] C. Allig and G. Wanielik, "Extending the vehicular network simulator artery in order to generate synthetic data for collective perception," *Advances in Radio Science*, vol. 17, pp. 189–196, 09 2019.

[2] J. Snider, "Automatic steering methods for autonomous automobile path tracking," 04 2011.

[3] N. Chowdhri, "Model predictive control for automated driving and collision avoidance: Design of an integrated nmpc with simultaneous lateral and longitudinal control via steering and braking," 2019.

[4] J. J. Breuer, "Analysis of driver-vehicle-interactions in an evasive manoeuvre-results of'moose test'studies," in *Proc. 16th ESV Conf., Paper*, no. 98-S2, 1998.

[5] J. Rawlings and D. Mayne, *Model Predictive Control: Theory and Design*. Nob Hill Publishing, 2008.